

Curvature effects in interfacial acidity of amphiphilic vesicles

Petch Khunpetch ^{1,2,*} Arghya Majee ^{3,†} Hu Ruixuan,² and Rudolf Podgornik ^{2,4,5,6}

¹Department of Physics, Faculty of Science, Ramkhamhaeng University, Bang Kapi, 10240 Bangkok, Thailand

²School of Physical Sciences, University of Chinese Academy of Sciences, 100049 Beijing, China

³Max Planck Institute for the Physics of Complex Systems, 01187 Dresden, Germany

⁴Kavli Institute for Theoretical Sciences, University of Chinese Academy of Sciences, 100049 Beijing, China

⁵CAS Key Laboratory of Soft Matter Physics, Institute of Physics, Chinese Academy of Sciences, 100190 Beijing, China

⁶Wenzhou Institute of the University of Chinese Academy of Sciences, Wenzhou, 325000 Zhejiang, China



(Received 30 March 2023; accepted 11 July 2023; published 7 August 2023)

We analyze the changes in the vicinal acidity (pH) at a spherical amphiphilic membrane. The membrane is assumed to contain solvent accessible, embedded, dissociable, charge-regulated moieties. Basing our approach on the linear Debye-Hückel approximation, as well as on the nonlinear Poisson-Boltzmann theory, together with the general Frumkin-Fowler-Guggenheim adsorption isotherm model of the charge-regulation process, we analyze and review the dependence of the local pH on the position, as well as bulk electrolyte concentration, bulk pH, and curvature of the amphiphilic single membrane vesicle. With appropriately chosen adsorption parameters of the charge-regulation model, we find a good agreement with the available experimental data.

DOI: [10.1103/PhysRevE.108.024402](https://doi.org/10.1103/PhysRevE.108.024402)

I. INTRODUCTION

The charging state of phospholipid membranes [1] and lipid nanoparticles [2], but also other amphiphilic [3] as well as proteinaceous self-assemblies [4], is governed by the protonation-deprotonation equilibria of dissociable surface molecular groups in contact with the aqueous subphase. In the case of proteins [5], the negative charges stem from the deprotonated carboxylate on the side chains of aspartic and glutamic acid, and the deprotonated hydroxyl of the phenyl group of tyrosine, while the positive charge originates from the protonated amine group of arginine and lysine, as well as the protonated secondary amine of histidine [6]. In the case of phospholipids, the negative charge is derived from deprotonated phosphate groups and deprotonated carboxylate, while the positive charge, though rare in naturally occurring lipids [7], stems from the protonated amine group or other titratable molecular moieties with an engineered dissociation constant [8].

Among the phenomena in biomolecular assemblies where charging equilibria are particularly important, one can specifically name the electrostatic interactions between membranes [9], ion transport across the membranes [10], as well as the insertion and translocation of membrane proteins [11]. To these well-known examples one could also add the emerging role of

charging equilibria in viral proteinaceous capsid shells [12], their interactions with various substrates [13], and structural reconstructions and maturation processes in chimeric protein-lipid capsid shells [14–16].

The charging equilibria in biomacromolecular assemblies typically involve local pH and local bathing solution ion concentrations, which—as has been recognized for a while—in general differ from the bulk conditions [6,17,18], implying that the changes in the bathing solution properties will affect not only the pH sensing and pH response of lipid membranes [19], but will also—and even more importantly—affect the membrane protein(s) entering different biochemical reactions required for the sustainability and proliferation of life. Elucidation of the quantitative details of the relation between *bulk* and *local* solution properties thus constitutes one of the challenges in the description of biomacromolecular assemblies.

We have recently formulated [20–22] a theoretical model that couples the full macroscopic continuum description of electrostatic interactions with the surface protonation and deprotonation reactions of charged lipids and/or other amphiphilic molecules [8]. This model not only yields the details of the lipid charging state as a function of the curvature and bathing solution parameters, such as pH and salt concentration, but also, and this will be the focus here, the full spatial profile of the pH in the vicinity of the membrane. In this way, we can connect the interfacial curvature with the interfacial pH for the nonplanar self-assemblies and assess the role of the surface curvature in the interfacial acidity and basicity properties. This connection in itself attests to the fact that the knowledge of the *bulk* bathing solution properties does not imply that we know what the *local* solution properties are, which, in the last instance, determine the solution state near the proteins and lipids functional groups. Below we will argue that the local pH can actually veer off quite far from the nominal values set in the bulk.

*petch.k@rumail.ru.ac.th; co-first and co-corresponding author

†majee@pks.mpg.de; co-first and co-corresponding author

In what follows, we will first recapitulate the basic features of our theoretical model with the Poisson-Boltzmann volume free energy functional for mobile charges and the Frumkin-Fowler-Guggenheim adsorption isotherm model, formulated in terms of the appropriate surface free energy, for the surface charging equilibrium. We then solve the model in the linearized Debye-Hückel (DH) approximation as well as in the full Poisson-Boltzmann (PB) theory for a spherical vesicle with finite thickness membrane, whose solvent accessible surfaces contains the dissociable moieties. We additionally assume that at all stages of the vesicle preparation, the mobile charges are equilibrated with the bulk characterized by a constant chemical potential. We specifically describe the spatial profiles of the vicinal as well as luminal pH as a function of the parameters of the model. Finally, we comment on the salient features of the interfacial acidity and its dependence on the bulk properties.

II. CHARGE-REGULATION MODEL

We consider a spherical vesicle with salt solution on the two sides of its bilayer membrane, composed of two charge-regulated (CR) monolayers containing dissociable moieties, as shown in Fig. 1. The inner radius of the vesicle shell is R with charge density σ_1 , and the outer radius is $R + w$ with charge density σ_2 . The approach described below broadly follows our previous work and we shall only list the relevant details that were further elaborated in Refs. [8,20–22]. We will focus on two CR models corresponding either to a symmetric surface charge density interval, $-\sigma_0 \leq \sigma_{1,2} \leq \sigma_0$ (model 1), or to an asymmetric surface charge density interval, $-\sigma_0 \leq \sigma_{1,2} \leq 0$ (model 2), where $\sigma_0 = e_0 n_0$ is a structural charge parameter corresponding to the maximal dissociated surface charge, with e_0 the elementary charge ($e_0 > 0$) and n_0 a structural surface density of dissociation sites. For all the results presented here, we use $n_0 = 1 \text{ nm}^{-2}$.

A fundamental quantity in our CR models is the fraction of the neutral lipid heads $\eta_{1,2} \in [0, 1]$ on the inner and outer monolayers, where the protonation-deprotonation of dissociable moieties can take place, and we assume that $\sigma_{1,2}$ and $\eta_{1,2}$ are uniform over the two monolayers. The connection between $\sigma_{1,2}$ and $\eta_{1,2}$ is different in the two models that we consider. In model 1 [20], the CR surface charge density is given by

$$\sigma_i = 2n_0 e_0 (\eta_i - \frac{1}{2}), \quad (1)$$

with $-e_0 n_0 \leq \sigma_{1,2} \leq e_0 n_0$ that can obviously change sign, while in model 2 [23], we assume that the CR surface charge density is given by

$$\sigma_i = n_0 e_0 (\eta_i - 1), \quad (2)$$

so that $-e_0 n_0 \leq \sigma_{1,2} \leq 0$ which, consequently, cannot change sign.

We note that the two models described by Eqs. (1) and (2) correspond to two situations, where the protonation-deprotonation of dissociable moieties can lead to positive or negative net charge (model 1), or it leads only to a single type of net charge (model 2). Model 1 would correspond to a membrane composed of at least two types of lipids, of which one can be deprotonated (negative) and another one that

can be protonated (positive), with the latter rarely occurring naturally [7]. Another instance would be a membrane with embedded proteins, which are naturally polyampholytes and contain both positive and negative amino acids, with the net charge of the protein-membrane complex depending on the pH. Model 2, on the other hand, is simpler and corresponds to a single type of dissociable surface group, prevalently negative in the case of naturally occurring lipids. Apart from being more complicated, model 1 needs, in general, more phenomenological parameters, a complication we bypass by simply assuming a single zwitterionic model characterized by Eq. (1) for numerical convenience.

In numerical calculations the static dielectric constant of water is assumed as $\epsilon_w = 80$ and that of the lipid bilayer membrane as $\epsilon_p = 5$. The Debye screening length ($\lambda_D = \kappa_D^{-1}$) varies from about 0.34 to 10.75 nm, corresponding to the monovalent salt concentration ranging from 1.0 to 0.001 M [24]. Moreover, we define $\mu = \epsilon_p / \epsilon_w$.

III. ELECTROSTATIC FREE ENERGY: POISSON-BOLTZMANN AND DEBYE-HÜCKEL FORMS

We start with the standard PB free energy, or the DH free energy in the linearized case, that depends on the distribution of mobile charges, assumed to belong to a univalent electrolyte with a fixed bulk chemical potential. The surface charges are assumed to be located at both interfaces of a spherical membrane. Most of our results pertain to the DH approximation that has proven to be useful not only to provide qualitative, but also quantitative results in the context of various problems involving interactions of charged colloidal particles [20,21,25–28]. We should, however, clearly state that the linearization implied by the DH approximation pertains only to electrostatics and not to the surface charging equilibrium, which is always considered in its full, nonlinear form.

There are various ways to write the PB free energy [29] and we choose the field description, with the radially varying mean-field electrostatic potential $\psi(r)$ as the only relevant variable. The total PB electrostatic free energy is then given by

$$\mathcal{F}_{ES} = - \int_V dV \left\{ \frac{\epsilon_w \epsilon_0}{2} \left(\frac{d\psi(r)}{dr} \right)^2 + 2n_l [\cosh \beta e_0 \psi(r) - 1] \right\} + \oint_{A_1} dA_1 \psi(R_1) \sigma_1 + \oint_{A_2} dA_2 \psi(R_2) \sigma_2, \quad (3)$$

where n_l is the univalent electrolyte concentration in the bulk, $R_1 = R$ and $R_2 = R + w$, while the equilibrium value of $\psi(r)$ is obtained from the corresponding Euler-Lagrange (EL) equation. The volume integral extends over all the regions except the bilayer interior. Within the bilayer interior, there are no mobile charges and the second term in the square brackets is absent, so that the electrostatic free energy is simply

$$\mathcal{F}_{ES} = - \frac{\epsilon_p \epsilon_0}{2} \int_V dV \left(\frac{d\psi(r)}{dr} \right)^2 + \oint_{A_1} dA_1 \psi(R_1) \sigma_1 + \oint_{A_2} dA_2 \psi(R_2) \sigma_2, \quad (4)$$

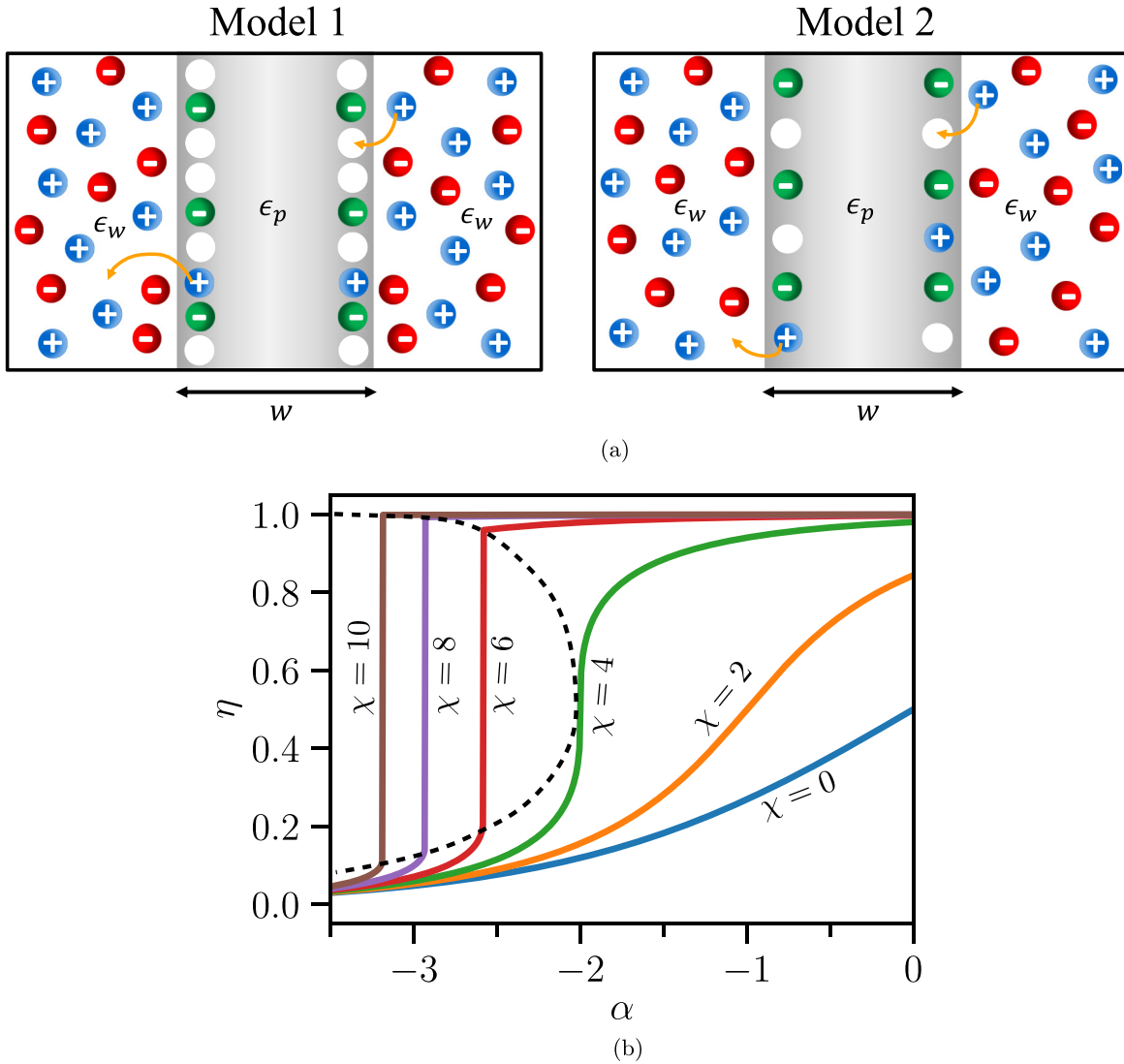


FIG. 1. (a) Schematic representations of the relevant features of the charge regulation at the surface of an amphiphilic bilayer within model 1 and model 2. The gray slabs correspond to the bilayer membrane of width w . The white circles represent the dissociable protonation and deprotonation sites on the bilayer surface; the green negative charges are the fixed surface charges. Blue ions are protons and red ions are mobile negative ions. Note the difference between the ratio of available CR surface sites to the amount of fixed negative charges (green): In model 1, this ratio equals 2, whereas in model 2, it equals 1. Consequently, in model 1, the charge is regulated in the interval $-\sigma_0 \leq \sigma_{1,2} \leq \sigma_0$ [see Eq. (1)], whereas in the case of model 2, it is regulated in the interval $-\sigma_0 \leq \sigma_{1,2} \leq 0$ [see Eq. (2)]. σ_0 is a fixed maximal structural charge density. Protons provided by the dissociable surface moieties can exchange with the solution and in the process charge or discharge the dissociable groups. (b) Solution of the Frumkin-Fowler-Guggenheim dissociation isotherm, given by Eq. (12), for a single charge-regulated monolayer with different values of the χ interaction parameter with $\psi = 0$. The critical isotherm corresponding to the inflection point of $\eta = \eta(\alpha)$ is given by $(\alpha, \chi) = (-2, 4)$, implying that for $\chi \leq 4$, $\eta(\alpha)$ is a smooth function of α , while for $\chi > 4$, $\eta(\alpha)$ displays a discontinuous first-order transition between a state with $\eta \simeq 0$ and a state $\eta \simeq 1$, delimited by the dashed coexistence line. $\chi = 0$ corresponds to the Langmuir isotherm with no discontinuous state transition.

where the volume integral now extends over the bilayer interior and, of course, the permittivity ϵ_p needs to be used.

A common approach to electrostatic effects in soft matter and specifically in the case of charged membrane vesicles is via the DH approximation [30], often coupled together with small curvature, second-order expansion [7,31,32]. In the DH approximation, valid strictly for $\beta e_0 \psi(r) \ll 1$ but yielding qualitatively similar results to the full PB solution also outside this limit [8], the corresponding expressions for the electrostatic free energy given by Eq. (3) simplify

considerably to

$$\mathcal{F}_{ES} = -\frac{\epsilon_w \epsilon_0}{2} \int_V dV \left[\left(\frac{d\psi(r)}{dr} \right)^2 + \kappa_D^2 \psi(r)^2 \right] + \oint_{A_1} dA_1 \psi(R_1) \sigma_1 + \oint_{A_2} dA_2 \psi(R_2) \sigma_2, \quad (5)$$

where the inverse square of the Debye screening length λ_D is given by $\kappa_D^2 = 2n_I \beta e_0^2 / (\epsilon_w \epsilon_0)$ and the volume integral again

extends over all the regions except the bilayer interior. While the free energies given by Eqs. (3) and (5) imply the PB and the DH equation in the regions accessible to electrolyte ions [25], respectively, Eq. (4) leads to the standard Laplace equation inside the lipid dielectric core. Inserting the solution of the EL equations back into Eq. (5), it is then further reduced to a form corresponding to the Casimir charging process [33],

$$\begin{aligned} \mathcal{F}_{ES}(\sigma_1, \sigma_2, R) &= 4\pi \sum_{i=1}^2 R_i^2 \int_0^{\sigma_i} d\sigma_i \psi(\sigma_1, \sigma_2, R_i) \\ &\longrightarrow \frac{1}{2} \sum_{i=1}^2 4\pi R_i^2 \sigma_i \psi(\sigma_1, \sigma_2, R_i), \end{aligned} \quad (6)$$

where the right arrow indicates the DH limit of the same expression where the potentials are linear functions of the charge density. With the explicit solution for the electrostatic potential (see Appendix A), we can derive the DH expression for the electrostatic free energy per area as a function of the radius of curvature R to inverse quadratic order [24], obtaining an approximate but highly accurate form of the free energy,

$$\begin{aligned} \frac{\kappa_D \epsilon_0 \epsilon_w \mathcal{F}_{el}(\sigma_1, \sigma_2, R)}{2\pi R^2} &= f_0(\sigma_1, \sigma_2, \kappa_D, w) + \frac{f_1(\sigma_1, \sigma_2, \kappa_D, w)}{\kappa_D R} \\ &+ \frac{f_2(\sigma_1, \sigma_2, \kappa_D, w)}{(\kappa_D R)^2}, \end{aligned} \quad (7)$$

where the curvature-independent terms, $f_0(\sigma_1, \sigma_2, \kappa_D, w)$, $f_1(\sigma_1, \sigma_2, \kappa_D, w)$, and $f_2(\sigma_1, \sigma_2, \kappa_D, w)$ are explicitly given in Appendix C. In general, the above free energy density of a curved membrane is not symmetric in the two solvent accessible surface charge densities that were assumed to be constant.

The DH electrostatic free energy for fixed surface charges displays a general quadratic dependence on the curvature of the lipid bilayer. This quadratic dependence of electrostatic free energy was standardly taken as a point of departure for the electrostatic renormalization of the mechanical properties of membranes, such as surface tension and bending rigidity [24,34–38], but ceases to be the case for charge-regulated membranes.

IV. CHARGE-REGULATION FREE ENERGY AND SELF-CONSISTENT BOUNDARY CONDITIONS

Assuming that the inner and outer membrane surfaces are chemically identical, we presume that the surface charge-regulation process can be described by the Frumkin-Fowler-Guggenheim adsorption isotherm, which is a two-parameter adsorption model [39], parameterized with the adsorption energy α , the interaction energy between adsorbed ions, χ , and the lattice gas entropy. For $\chi = 0$, the Frumkin-Fowler-Guggenheim model reduces to the Langmuir model. Other, multiparametric models of variable complexity can be defined, but will not be analyzed here [40].

The corresponding charge-regulation free energy densities of the inner and outer membrane surfaces, denoted by

$i = 1, 2$, are given by

$$\begin{aligned} \frac{\mathcal{F}_{CR}(\eta_i)}{4\pi R_i^2} &= n_0 k_B T \left[-\alpha \eta_i - \frac{\chi}{2} \eta_i^2 + \eta_i \ln \eta_i \right. \\ &\left. + (1 - \eta_i) \ln(1 - \eta_i) \right]. \end{aligned} \quad (8)$$

This can be further normalized with respect to the inner area $4\pi R^2$, which is used later. The first two terms in the free energy are enthalpic in origin. The other terms are the lattice gas mixing entropy of charged sites with the surface area fraction η and neutralized sites with the surface area fraction $1 - \eta$.

In the case of phospholipids such as phosphatidic acid (PA; smallest and simplest phospholipid; precursor for other phospholipids), phosphatidylserine (PS), and phosphatidylglycerol (DPPG), the negative charge comes from the deprotonated conjugate base of phosphoric acid and deprotonated carboxylate, while the positive charge comes from the protonated amine or ammonium head of cationic lipids but can also be substituted with an engineered dissociation constant [1,41].

In these cases of charge regulation, the adsorbing and desorbing particles are identified as protons and α is then the deprotonation free energy difference [42], which, in the case of the Langmuir adsorption model [23], becomes

$$\alpha = (\text{p}K_a - \text{pH}^0) \ln 10, \quad (9)$$

where $\text{p}K_a$ is the dissociation constant of the deprotonation reaction and $\text{pH}^0 = -\log_{10} [\text{H}^+]$ is the bulk acidity. The above identity is valid only on the mean-field level and if the concentrations of H^+ and OH^- ions, corresponding to the pH value, are much lower than the concentration of the added salt.

The Langmuir model in this context is equivalent to a Henderson-Hasselbalch equation with electrostatics included [43]. Furthermore, χ , as in the related lattice regular solutions theories (e.g., the Flory-Huggins theory [44]), describes the short-range interactions between nearest-neighbor (de)protonation sites [45]. A parameter value $\alpha \leq 0$ encodes a favorable adsorption free energy, while $\alpha \geq 0$ represents the tendency of particles on the macro-ion surface adsorption sites to phase separate into domains. Figure 1 displays a schematic depiction of the charge-regulation process and the Frumkin-Fowler-Guggenheim adsorption isotherm as a function of α for different values of the interaction parameter χ . It is important to reiterate at this point that other charge-regulation models are, of course, possible and have been proposed for various dissociable groups in different contexts [39,40,46]. Our reasoning in choosing the particular Frumkin-Fowler-Guggenheim dissociation isotherm was guided by its simplicity in the way it takes into account the salient features of the dissociation process on the membrane surface, and the fact that the implied phenomenology has been analyzed before in the context of charged amphiphilic systems [47].

From the general electrostatic free energy given by Eq. (6), we then obtain the surface electrostatic potential as

$$\frac{\partial \mathcal{F}_{ES}(\sigma_1, \sigma_2, R)}{\partial \sigma_i} = 4\pi R_i^2 \psi(\sigma_1, \sigma_2, R_i), \quad (10)$$

for $i = 1, 2$. By considering Eqs. (10), as well as the form of the charge-regulation free energy given by Eq. (8), we

derive the standard Frumkin-Fowler-Guggenheim adsorption isotherm [39,46] from the thermodynamic equilibrium obtained by minimizing the total free energy of the system. We get two equations that correspond to charge-regulation boundary conditions,

$$\frac{\partial \mathcal{F}_{ES}(\sigma_1, \sigma_2, R)}{\partial \sigma_i} \frac{\partial \sigma_i}{\partial \eta_i} + \frac{\partial \mathcal{F}_{CR}(\eta_i)}{\partial \eta_i} = 0, \quad (11)$$

for $i = 1, 2$, which, by taking into account Eq. (10), can be solved by an implicit equation for $\eta_i = \eta_i(\psi)$ [20,21,45,48] in the form

$$\eta_i(\psi) = (1 + e^{-\alpha - \chi \eta_i(\psi) + 2\beta e_0 \psi})^{-1}, \quad (12)$$

with $\eta_i(\psi) = \eta_i[\psi(\sigma_1, \sigma_2, R_i)]$. The numerical solution of the above equation is presented in Fig. 1 and corresponds to the Frumkin-Fowler-Guggenheim adsorption isotherm. Again, we reiterate that the DH linearization pertains only to electrostatics, i.e., the first term in Eq. (11), while the surface charging equilibrium is always considered in its full, nonlinear form. It is evident from Fig. 1 that for $\chi \leq -2\alpha$, the adsorption isotherm exhibits a discontinuous transition, whereas above the ‘‘critical isotherm,’’ $\chi = -2\alpha$, i.e., $\chi \geq -2\alpha$, it remains continuous.

The boundary condition derived above, given by Eq. (11), together with the solution of either the full PB equation or the linearized DH version for the electrostatic free energy, given by Eq. (7), constitute the basic equations of our model. In the case of the linear theory with the electrostatic free energy given by Eq. (7), we obtain the surface potentials from Eq. (10) as $\psi(R_i) = \psi_i(\eta_1, \eta_2)$.

Finally, we should note that our approach is based on the free energy of the CR process and not on the assumed isotherms that would follow from some chemical equilibrium considerations, as was often done in the literature [23]. While the two approaches are, in principle, equivalent, it seems to us that the free energy approach has a more universal appeal and also allows the explicit calculation of the total free energy, i.e., ES plus CR.

V. COMPARISON BETWEEN THE FULL PB AND THE APPROXIMATE DH SOLUTIONS

The DH approximation [30] is standardly invoked in order to derive limiting expressions and analytical formulas in various contexts of macromolecular electrostatics [27,28]. In order to be able to substantiate our usage of the DH approximation for most of the numerical results, we compare the pH profile resulting from the full PB equation with the consequences of the linearized DH equation. Again, we point out that the linearization applies only to the electrostatic part, but not to the charge-regulation part. Sometimes the linearization is also extended to that case of charge regulation [49], as in the constant regulation boundary condition often invoked by Borkovec *et al.* [50], where for large separations one may expand the charge-potential relationships at the surface around the potential at infinite separation.

We quantitatively compare the PB and the DH results for certain choices of the model parameters in Appendix B. The general conclusion is that qualitatively, and also often quantitatively, they generally coincide but exhibit differences in

certain parts of the parameter space. It seems that one can thus safely use the DH approximation if the focus is on the qualitative features, whereas a PB-based calculation would be needed in order to do quantitative comparisons.

VI. INTERFACIAL AND LUMINAL pH

The above derivation and, specifically, the definition $\alpha = (\text{p}K_a - \text{pH}) \ln 10$ assume that the concentration of the protons in solution is much lower than the concentration of salt and does not contribute to the spatial profile of the electrostatic potential, either on the PB or the DH level. For many dissociable moieties at physiological solution conditions, this assumption holds well, but, in general, a more detailed implementation of the pH effects is needed; see, e.g., Refs. [51,52].

With the above provisos, the local pH is a ‘‘passive’’ variable in the solution, except at the surface of the lipid bilayer where it determines the dissociation state. The spatial dependence of $\text{pH} = -\log_{10} [\text{H}^+]$ is obtained from the electrostatic potential as

$$\begin{aligned} \text{pH}(r) &= -\log_{10} [\text{H}^+(r)] \\ &= -\log_{10} [\text{H}^+]_0 + \beta e_0 \psi(r) \log_{10} e \\ &= \text{pH}^0 + \beta e_0 \psi(r) \log_{10} e, \end{aligned} \quad (13)$$

where $\text{pH}^0 = -\log_{10} [\text{H}^+]_0$ is either the pH in the outside bulk reservoir or the inside pH that is set by the procedure of vesicle preparation and can coincide with or be different from the bulk value [53]. The calculation of $\text{pH}(r)$ then follows from the electrostatic potential profile that is written explicitly in the DH approximation in Appendix A, yielding the pH profile in the interior of the vesicle as

$$\text{pH}(r \leq R) = -\log_{10} [\text{H}^+]_0 + \beta e_0 \log_{10} e A \frac{\sinh(\kappa_D r)}{r}, \quad (14)$$

where κ_D is the inverse Debye length and A is given in Appendix A. Outside the vesicle, the relevant dependence is obtained as

$$\text{pH}(r \geq R) = -\log_{10} [\text{H}^+]_0 + \beta e_0 \log_{10} e B \frac{\exp(-\kappa_D r)}{r}, \quad (15)$$

with B given in Appendix A. Obviously, both inside as well as outside the vesicle, the local pH decays with the Debye length. The two constants $A = A(\sigma_1, \sigma_2, \kappa_D w, \kappa_D R)$ and $B(\sigma_1, \sigma_2, \kappa_D w, \kappa_D R)$ are linear functions of the internal and external surface membrane charge densities. The above formulas allow us to explicitly obtain the spatial variation of pH around and across the membrane, as well as the drops in pH either across the membrane or between the bulk reservoir and the region adjacent to the membrane.

Note that while the electrostatic potential is also well defined inside the membrane, the pH is not since the protons do not move freely across the hydrophobic kernel of the membrane.

Because the pH exhibits a spatially varying profile, $\text{pH} = \text{pH}(r)$, we can define different characteristic values that can be, at least in some cases, obtained either directly or indirectly from experiments [11,54]. First, we can define a drop in pH

across the membrane of the vesicle of magnitude

$$\Delta pH_m = pH(R + w) - pH(R). \quad (16)$$

Two other important quantifiers are the difference between the bulk pH^0 and pH right at the outer surface as a function of the outer radius of the vesicle R , defined as

$$\Delta pH_{out} = pH(R + w) - pH^0. \quad (17)$$

Similarly, the difference between the bulk value pH^0 and pH right at the inner surface as a function of the inner radius of the vesicle R is defined as

$$\Delta pH_{in} = pH(R) - pH^0. \quad (18)$$

$$\lim_{r \rightarrow 0} \psi(r) = \psi(0) = \frac{\epsilon_w \sigma_1 R^2 \kappa_D w^2 + \epsilon_p [\sigma_1 R^2 + \sigma_2 (R + w)^2] R + \epsilon_w \sigma_1 (1 + \kappa_D R) w R^2}{\epsilon_0 \epsilon_w \{(\epsilon_p - \epsilon_w) w^2 + \epsilon_p R^2\}} \text{csch}(\kappa_D R), \quad (19)$$

taking into account Appendix A. The pH in the lumen then follows as

$$pH(0) = -\log_{10} [H^+]_0 + \beta e_0 \log_{10} e \psi(0), \quad (20)$$

where $\log_{10} [H^+]_0$ is the acidity in the bulk reservoir. The expression for $pH(0)$ has two well-defined limits defined by

$$\lim_{\kappa_D R \ll 1} \psi(0) = \frac{\epsilon_p [\sigma_1 R^2 + \sigma_2 (R + w)^2] + \epsilon_w \sigma_1 w R}{\epsilon_0 \epsilon_w \{(\epsilon_p - \epsilon_w) \kappa_D w^2 + \epsilon_p \kappa_D R^2\}} \quad (21)$$

and

$$\lim_{\kappa_D R \gg 1} \psi(0) = \frac{\epsilon_w \sigma_1 R (R + w) 2(\kappa_D R) (\kappa_D w) e^{-\kappa_D R}}{\epsilon_0 \epsilon_w \{(\epsilon_p - \epsilon_w) \kappa_D w^2 + \epsilon_p \kappa_D R^2\}}. \quad (22)$$

Clearly, in the second limit of $\kappa_D R \gg 1$, the potential in the center of the vesicle vanishes and thus the luminal pH is the same as in the bulk, if the membrane is fully permeable to all mobile charged species. Interestingly enough, as can be discerned from numerical solution, the electrostatic potential and, consequently, the pH inside the vesicle are almost constant up to the inner surface, implying that the Donnan potential approximation could be used for that case [55]. These are the only analytical limits that one can derive for this problem.

Finally, we note that our calculation is based on the chemical equilibrium and ionic identity between the ionic solution inside and outside the vesicle.

VII. RESULTS

We now analyze some numerical results obtained mostly within our model (1), unless specifically annotated for model (2).

We first investigate the full spatial profile of pH in the vicinity of the vesicle. We assume that in the preparation of the vesicle, the inner and the outer solutions are equilibrated at the same bathing solution pH . On the DH level, the solution for the potential can be derived analytically (see Appendix A), but the solution of the CR isotherm, given by Eq. (11), can only be obtained numerically. The latter then yields the two surface charge densities, $\sigma_{1,2}$. Figures 2 and 3 show the plots

of pH vs r obtained from Eq. (13) for different values of the bulk pH^0 and the CR parameters α , χ . Clearly, the general dependence of $pH(r)$ indicates a large variation close to both surfaces of the bilayer, to be quantified below.

We have used typical system parameters such as an inverse Debye length $\kappa_D = 1.215 \text{ nm}^{-1}$ or, equivalently, screening length $\lambda_D = 0.823 \text{ nm}$ corresponding to an aqueous electrolyte solution with 140 mM salt concentration. The dimensionless curvature h is defined as $h = 1/(\kappa_D R)$, where R is the inner radius of the vesicle. In Figs. 2 and 3, the dimensionless curvature h is fixed at 0.05, corresponding to $R = 16.46 \text{ nm}$.

From our Frumkin-Fowler-Guggenheim charge-regulation model, we obtain $(\sigma_1 = -0.202 e_0/\text{nm}^2, \sigma_2 = -0.395 e_0/\text{nm}^2)$ for $(\alpha = -5, \chi = 0)$ (no surface interaction) [Fig. 2(a)] and $(\sigma_1 = -0.233 e_0/\text{nm}^2, \sigma_2 = -0.561 e_0/\text{nm}^2)$ for $(\alpha = -10, \chi = 10)$ [Fig. 2(b)]. The plots show that the pH decreases remarkably at the region close to the vesicle's inner surface and that the pH at the outer surface is lower than that at the inner surface. In general, the pH exponentially approaches the bulk pH^0 away from the membrane. For the negative $\alpha = -10$ and $\chi = 20$ ($\chi = -2\alpha$) case [Fig. 2(c)], the Frumkin-Fowler-Guggenheim charge-regulation model yields $(\sigma_1 = 0.011 e_0/\text{nm}^2, \sigma_2 = -0.561 e_0/\text{nm}^2)$. Close to the surface, the pH increases like $\sinh(\kappa_D r)$, which is shown with more detail in Fig. 2(d).

For positive $\alpha > 0$ (Fig. 3), we obtain $(\sigma_1 = 1.357 e_0/\text{nm}^2, \sigma_2 = 0.567 e_0/\text{nm}^2)$ at $(\alpha = 20, \chi = 20)$ [Fig. 3(a)] and $(\sigma_1 = 0.474 e_0/\text{nm}^2, \sigma_2 = 0.567 e_0/\text{nm}^2)$ at $(\alpha = 5, \chi = 10)$ [Fig. 3(b)]. All curves exhibit the same scaling $\sinh(\kappa_D r)$ near the inner surface. Clearly, in the case of $\alpha > 0$, the local pH decreases from the value it attains near the surface of the bilayer towards the bulk pH^0 for both Figs. 3(a) and 3(b).

In order to clearly see the deviation of pH from the bulk pH^0 , we have used $\kappa_D = 1/20 \text{ nm}^{-1}$ and $R = 10 \text{ nm}$ with dimensionless curvature h fixed at 2. Figure 4 presents the plot of $pH(r)$ across the membrane for bulk $pH^0 = 5.0$, $(\alpha, \chi) = (10, 10)$ [Fig. 4(a)], $(\alpha, \chi) = (-10, 0)$ [Fig. 4(b)]. The

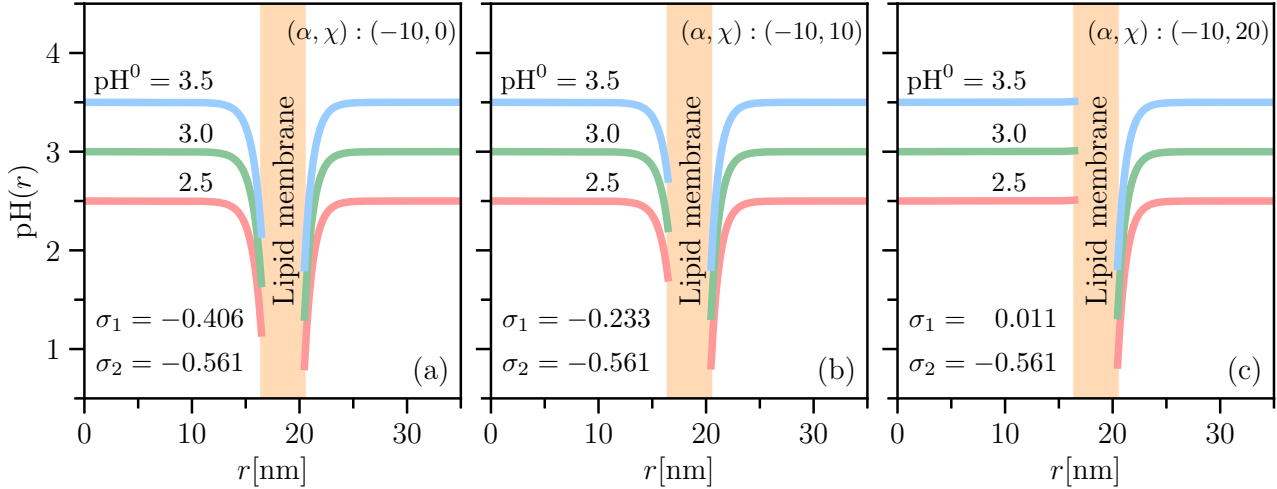


FIG. 2. Plot of $\text{pH}(r)$ across the membrane for different values of bulk pH^0 , in the case of (a) Langmuir dissociation isotherm $(\alpha, \chi) = (-10, 0)$ and (b), (c) two Frumkin-Fowler-Guggenheim dissociation isotherms for (b) $(\alpha, \chi) = (-10, 10)$ and (c) $(\alpha, \chi) = (-10, 20)$, at negative values of α . $\sigma_{1,2}$ indicate the values of the inner or outer surface charge densities in the unit of e_0/nm^2 corresponding to the chosen values of (α, χ) . In all cases, $n_0 = 1 \text{ nm}^{-2}$, $\kappa_D = 1.215 \text{ nm}^{-1}$, and $R = 16.46 \text{ nm}$, with dimensionless curvature h fixed at 0.05. The Bjerrum length $\ell_B = 0.74 \text{ nm}$, $\epsilon_p = 5$, $\epsilon_w = 80$, surface dissociable group concentration $n_0 = 1 \text{ nm}^{-2}$, and $w = 4 \text{ nm}$. σ_1 and σ_2 are obtained from the CR process. All curves show that the pH vicinal to the bilayer reduces remarkably from pH^0 in the bulk, except in (c) where this is the case only for pH in the outer compartment. pH at the outer surface is typically lower than right at the inner surface and then increases exponentially towards pH^0 in the region far from the outer surface. The $\text{pH}(r)$ for the Frumkin-Fowler-Guggenheim dissociation isotherm $(\alpha, \chi) = (-10, 20)$ in (c) is mostly independent of the position, except in the immediate vicinity of the inner surface, but is unobservable on the scale of the figure. Note that σ_2 does not change to the numerical accuracy of the first three decimal places.

rightmost panels show the expanded $\text{pH}(r)$ scale in order to see the small changes with r . The vicinal pH close to the outer surface of the vesicle can be drastically different from the bulk one, depending on the parameters.

We now analyze the dependence of the $\Delta\text{pH}_{\text{out}}$ on the various parameters of the system in Figs. 5 and 6. The procedure is the same as before; we solve analytically for the electrostatic potential and then obtain the corresponding surface charges from the Frumkin-Fowler-Guggenheim

charge-regulation model. The inverse Debye length is set as $\kappa_D = 1.215 \text{ nm}^{-1}$. Of particular importance is the dependence on the curvature and radius of the bilayer. In Figs. 5 and 6, we show this dependence for positive and negative α . Clearly, at first, $\Delta\text{pH}_{\text{out}}$ starts with a positive value, meaning that the surface pH is larger than the bulk pH^0 . It then increases with the radius, reaches a maximum, and then decays, eventually even turning negative. This behavior is the more pronounced the more α is negative. For positive values of α , $\Delta\text{pH}_{\text{out}}$ starts

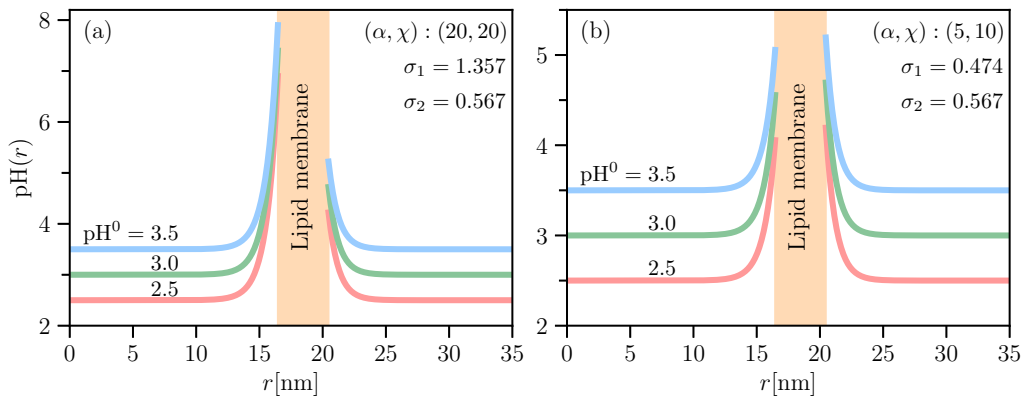


FIG. 3. Plot of the difference in the behavior of $\text{pH}(r)$ across the membrane in the case of a (a) Frumkin-Fowler-Guggenheim dissociation isotherm $(\alpha, \chi) = (20, 20)$ and (b) Langmuir dissociation isotherm $(\alpha, \chi) = (5, 10)$, at positive values of α . $\sigma_{1,2}$ indicate the values of the inner or outer surface charge density in the unit of e_0/nm^2 corresponding to the chosen values of (α, χ) . In all cases, $n_0 = 1 \text{ nm}^{-2}$, $\kappa_D = 1.215 \text{ nm}^{-1}$, and $h = (\kappa_D R)^{-1} = 0.05$. All curves show that at the region close to the inner surface of the vesicle, the pH increases as $\sinh(\kappa_D r)$. The pH decreases exponentially towards pH^0 in the region far from the outer surface for both (a) and (b). The Bjerrum length $\ell_B = 0.74 \text{ nm}$, $\epsilon_p = 5$, $\epsilon_w = 80$, surface dissociable group concentration $n_0 = 1 \text{ nm}^{-2}$, and $w = 4 \text{ nm}$.

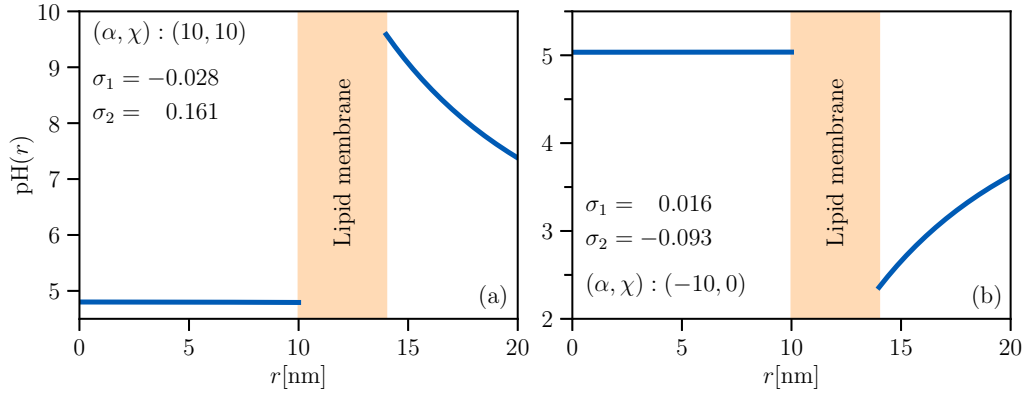


FIG. 4. Plot of $\text{pH}(r)$ across the membrane for bulk $\text{pH}^0 = 5.0$, (a) $(\alpha, \chi) = (10, 10)$, (b) $(\alpha, \chi) = (-10, 0)$. In both cases, $n_0 = 1 \text{ nm}^{-2}$, $\kappa_D = 1/20 \text{ nm}^{-1}$, and $R = 10 \text{ nm}$ with dimensionless curvature h fixed at 2. σ_1 and σ_2 , mentioned in the unit of e_0/nm^2 , are obtained from the CR process and correspond to the values of (α, χ) combination. The vicinal pH close to the outer surface of the vesicle can be drastically different from the bulk one, depending on the parameters, while the variation on the inner side cannot be discerned on the scale of the figure. The Bjerrum length $\ell_B = 0.74 \text{ nm}$, $\epsilon_p = 5$, $\epsilon_w = 80$, surface dissociable group concentration $n_0 = 1 \text{ nm}^{-2}$, and $w = 4 \text{ nm}$.

with a negative value, reaches a minimum, and then increases, eventually turning positive. Interestingly enough, because of the properties of the Frumkin-Fowler-Guggenheim dissociation isotherm, for small curvatures, $\Delta\text{pH}_{\text{out}}$ can start at zero [see Fig. 6(a)], for certain negative values of α . This simply means that at that α , the bilayer is uncharged, charges up at a critical value of curvature, and then follows basically the same behavior as for other negative values of α . The pronounced

variation of $\Delta\text{pH}_{\text{out}}$, which is, in principle, measurable [11], indicates that one could get some indication for the numerical values of the model parameters by comparing with suitable experiments.

In a recent detailed experimental work on detection of curvature-dependent interfacial pH for amphiphilic self-assemblies and unilamellar phospholipid vesicles, an interface-interacting spiro-rhodamine pH probe and Schiff

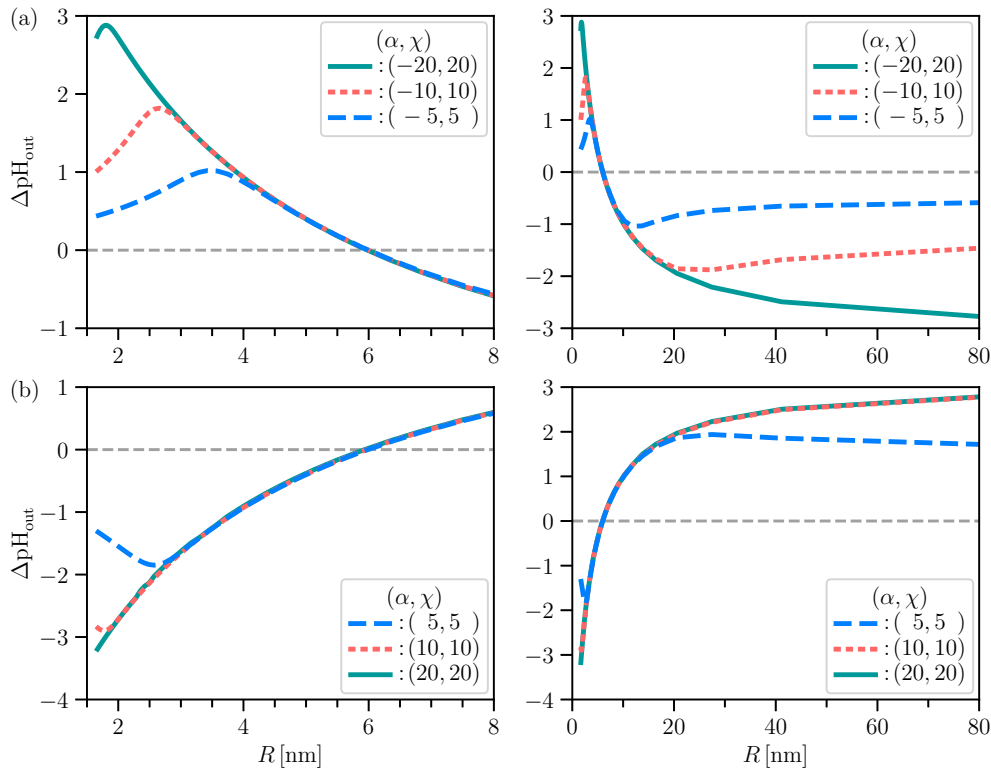


FIG. 5. Plot of $\Delta\text{pH}_{\text{out}}$ as defined in Eq. (17) vs R with $\kappa_D = 1.215 \text{ nm}^{-1}$ for different values of the CR parameters (α, χ) . (a) $\alpha \leq 0$ and (b) $\alpha > 0$ for small (left panels) and large (right panels) radii R . Clearly, the pH vicinal but exterior to the vesicle can be larger or smaller than the bulk pH^0 , depending on the charge-regulation parameters entering into the CR model. In general, $\alpha \leq 0$ makes the vicinal pH larger, while $\alpha \geq 0$ makes it smaller. Also, the larger χ , the larger is this effect.

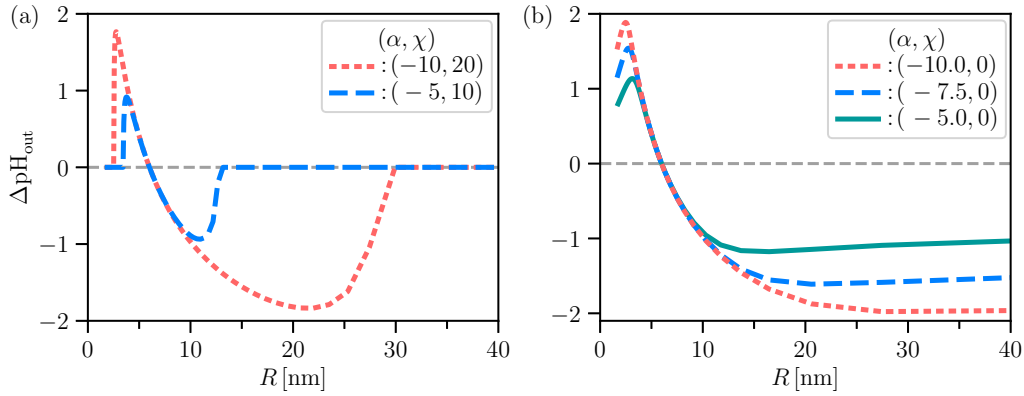


FIG. 6. Plot of $\Delta \text{pH}_{\text{out}}$ vs R for different values of the CR parameters (α, χ) and $\kappa_D = 1.215 \text{ nm}^{-1}$. (a) $\chi = -2\alpha$. (b) $\alpha < 0$ and $\chi = 0$ (no surface interaction). For large enough positive χ , the dependence of $\Delta \text{pH}_{\text{out}}$ on R shows a behavior akin to a second-order transition, where for small radii it vanishes, and then, at a critical value $R = R_c$, it starts deviating from zero, reaching for a maximum and then leveling off at a constant value for a sufficiently large R dependent on the values of the dissociation parameters (α, χ) . No such behavior is observed for the Langmuir dissociation isotherm $\chi = 0$.

base polarity probe have been used to measure the deviation of the local interfacial pH from the bulk phase [11]. It has been shown that the charging state (and polarity) of the amphiphile and phospholipid self-assemblies can be regulated by the curvature of the vesicle or micelle. While the experimental system is more complicated than our model and specifically contains also the interfacial dielectric constant, we believe it could be instructive to compare the predictions of our model with the measured values for $\Delta \text{pH}_{\text{out}}$.

We calculated $\text{pH}(r = R)$ and $\text{pH}(r = R + w)$ from the Frumkin-Fowler-Guggenheim CR model as described in detail above. The curvature radius R is set as 100 nm, which is one of the experimentally chosen values for the large unilamellar phospholipid vesicles in the experiment [11]. Other examples include radii $\sim 15, 25, 50$ nm that we did not explicitly consider. We assumed the bulk value $\text{pH}^0 = 5.2$ corresponding to the 2.0 mM cacodylate-HCl buffer. The inverse ionic screening length was taken as $\kappa_D = 0.5 \text{ nm}^{-1}$ (Table I) and $\kappa_D = 1.0 \text{ nm}^{-1}$ (Table II), corresponding to ionic concentrations of 25 and 100 mM. For both choices, $\text{pH}(r = R)$ and $\text{pH}(r = R + w)$ are larger than the bulk pH^0 for $\alpha > 0$ and less than the bulk pH^0 for $\alpha < 0$. In addition, for the

critical adsorption isotherm $\chi = -2\alpha$, we have $\text{pH}(r = R) = \text{pH}(r = R + w) = \text{pH}^0$ for small radii of curvature.

In experiments of Ref. [11] performed for 1,2-dimyristoyl-sn-glycero-3-phosphorylglycerol (DMPG)/1,2-dimyristoyl-sn-glycero-3-phosphocholine (DMPC) (2 : 1) mixture in the case of large unilamellar vesicles, the authors obtained $\Delta \text{pH}_{\text{out}} \simeq -1.4$ to -1.6 . In this particular case, the negative charge stems from the deprotonation of DMPG, while the DMPC lipid component carries no net charge. We model this situation both in the framework of model (1), as well as model (2), which seems to be the more realistic case. From our calculations in the framework of model (1), with $(\alpha, \chi) = (-10, 10)$, we obtain $\Delta \text{pH}_{\text{out}}$ [defined in Eq. (17)] as -1.221 (Table I) and -1.354 (Table II). Theoretically, depending on the combination of (α, χ) , the value of $\Delta \text{pH}_{\text{out}}$ from our model 1 could be obtained in the range of the experiments.

On the other hand, model 2 (Fig. 7), yielding only negative values of the surface charge density and thus, as already stated, being closer to the experimental situation corresponding to DMPG deprotonation, with $(\alpha, \chi) = (-5, 0)$ and $(\alpha, \chi) = (-5, 10)$, yields $\Delta \text{pH}_{\text{out}}$ up to -1.5 , which is again close to the stated experimental value [11]. Note, also,

TABLE I. pH at the inner and outer surfaces of the vesicle. The bulk pH^0 is set as 5.2. The radii of the vesicle are 50 nm and 100 nm. The Bjerrum length $\ell_B = 0.74 \text{ nm}$, $\epsilon_p = 5$, $\epsilon_w = 80$, surface dissociable group concentration $n_0 = 1 \text{ nm}^{-2}$, and $w = 4 \text{ nm}$. The inverse Debye length is $\kappa_D = 0.5 \text{ nm}^{-1}$.

(α, χ)	$R = 50 \text{ nm}$				$R = 100 \text{ nm}$			
	$\sigma_1(e_0/\text{nm}^2)$	$\sigma_2(e_0/\text{nm}^2)$	$\text{pH}(r = R)$	$\text{pH}(r = R + w)$	$\sigma_1(e_0/\text{nm}^2)$	$\sigma_2(e_0/\text{nm}^2)$	$\text{pH}(r = R)$	$\text{pH}(r = R + w)$
(10,0)	0.213	0.306	6.897	7.421	0.232	0.280	7.003	7.268
(10,20)	0.518	0.832	9.345	11.218	0.587	0.777	9.767	10.930
(20,20)	0.786	0.846	11.395	11.372	0.876	0.921	11.961	12.035
(20,10)	0.585	0.833	9.856	11.234	0.646	0.797	10.218	11.091
(-5,10)	0	0	5.2	5.2	0	0	5.2	5.2
(-10,20)	0	0	5.2	5.2	0	0	5.2	5.2
(-10,10)	-0.117	-0.188	4.265	3.840	-0.130	-0.165	4.190	3.979
(-20,5)	-0.390	-0.582	2.091	0.987	-0.429	-0.526	1.871	1.310

TABLE II. pH at the inner and outer surfaces of the vesicle. The bulk pH^0 is set as 5.2. The radii of the vesicle are 50 nm and 100 nm. The Bjerrum length $\ell_B = 0.74$ nm, $\epsilon_p = 5$, $\epsilon_w = 80$, surface dissociable group concentration $n_0 = 1$ nm $^{-2}$, and $w = 4$ nm. The inverse Debye length is $\kappa_D = 1.0$ nm $^{-1}$.

(α, χ)	$R = 50$ nm				$R = 100$ nm			
	$\sigma_1(e_0/\text{nm}^2)$	$\sigma_2(e_0/\text{nm}^2)$	$\text{pH}(r=R)$	$\text{pH}(r=R+w)$	$\sigma_1(e_0/\text{nm}^2)$	$\sigma_2(e_0/\text{nm}^2)$	$\text{pH}(r=R)$	$\text{pH}(r=R+w)$
(5,5)	0.346	0.495	6.545	7.032	0.376	0.452	6.641	6.889
(10,0)	0.420	0.549	6.828	7.232	0.449	0.515	6.918	7.128
(10,20)	1.139	0.846	9.575	8.359	1.078	0.922	9.307	8.662
(20,10)	1.140	0.846	9.578	8.359	1.078	0.922	9.307	8.662
(-5,10)	0	0	5.2	5.2	0	0	5.2	5.2
(-10,20)	0	0	5.2	5.2	0	0	5.2	5.2
(-10,10)	-0.256	-0.415	4.203	3.667	-0.284	-0.362	4.111	3.846
(-15,10)	-0.511	-0.754	3.215	2.412	-0.563	-0.697	3.040	2.595

that in model 2, the corresponding CR parameters (α, χ) corresponding to a close match with the experimental data are much smaller and thus possibly more realistic.

VIII. DISCUSSION

The properties of the bulk bathing solution can be quite different from the local environment near the embedded membrane proteins and lipid functional groups. This is in particular important for the spatial dependence of the acidity or basicity that actually governs the dissociation equilibrium of protein and lipid dissociable groups. Recent detailed experiments [11,54] have, in fact, shown that the surface pH can differ from the bulk one by several units. A deviation of 1.8 and 2.2 units from the bulk to the interface was detected for cationic cetrimonium bromide (CTAB) micelles and dimethyldioctadecylammonium bromide (DDAB) unilamellar vesicles [54], and the pH deviation of -1.4 to -1.6 for DMPG/DMPC (2 : 1) mixture large unilamellar vesicles [11], respectively.

Motivated by these experimental findings, we performed a detailed theoretical study of the effects of interfacial curvature in the case of bilayer vesicles with surface dissociable groups, on the interfacial acidity and basicity properties and found that the local pH can actually veer off quite far from the nominal values set in the bulk. Our theoretical model is based on the Poisson-Boltzmann volume free energy functional for mobile charges and the Frumkin-Fowler-Guggenheim adsorption isotherm model, formulated in terms of the appropriate surface free energy, for the surface dissociation equilibrium. It quantifies the surface adsorption and dissociation energy, the nearest-neighbor surface interaction energy, and the lattice gas entropy of adsorption and dissociation sites. In general, the model is rich enough to encode the simple Langmuir isotherm behavior also captured by the original charge-regulation model [23], as well as the more nuanced behavior of the Frumkin-Fowler-Guggenheim isotherm [20] and the ensuing first-order adsorption-dissociation transition; see Fig. 1. We solved the model numerically on the full nonlinear PB level as well as in the linearized DH approximation for

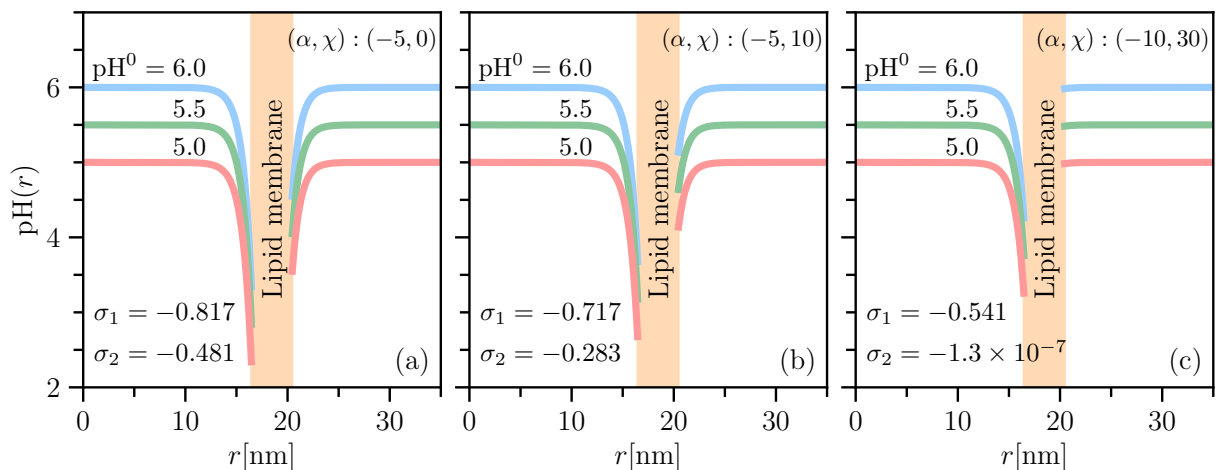


FIG. 7. Plot of $\text{pH}(r)$ across the membrane for model 2, given by Eq. (2), with $n_0 = 1$ nm $^{-2}$, $\kappa_D = 1.215$ nm $^{-1}$, and $R = 16.46$ nm, with dimensionless curvature h set at 0.05. The surface charge densities on both sides of the bilayer σ_1 and σ_2 are negative and are noted in the respective panels in the unit of e_0/nm^2 . For the Langmuir dissociation isotherm $(\alpha, \chi) = (-5, 0)$ or for the Frumkin-Fowler-Guggenheim dissociation isotherm $(\alpha, \chi) = (-5, 10)$, the corresponding $\Delta\text{pH}_{\text{out}}$ is comparable. For $(\alpha, \chi) = (-10, 30)$, $\Delta\text{pH}_{\text{out}}$ is much smaller and the deviation of pH from pH^0 at the outer surface can only be seen clearly after magnification in the immediate vicinity of the outer surface (not shown).

a spherical vesicle with finite thickness permeable membrane, whose solvent accessible surfaces contain the dissociable moieties. We were specifically interested to derive the spatial profiles of the vicinal as well as luminal pH as a function of the parameters of the model.

The numerical solutions of our model predict the full spatial dependence of pH as a function of surface dissociation model parameters, α and χ , assumed to be the same for the outer (solution interface) as well as inner (luminal interface) bilayer surface. What is clear is that for $\alpha \leq 0$, the pH vicinal to the bilayer differs remarkably from pH^0 of the bulk, with pH at the outer surface being lower than that right at the inner surface; see Fig. 2. This behavior can be modified by the amount of salt in the bulk reservoir or, equivalently, its screening length κ_D^{-1} , which can be seen by comparing the behavior of Figs. 2 and 4. As for the case of $\alpha \geq 0$ (see Fig. 3), clearly the pH at the luminal interface is much more perturbed than at the solution interface, implying that the negative curvature quantitatively has a larger effect than the positive curvature of the interface.

We also compared two different models of the CR process, one associated with a symmetric charge distribution across the bilayer (model 1) and another one with an asymmetric distribution (model 2). We note that the obtained pH profiles can be similar; the CR parameters (α , χ) corresponding to that profile are quite different; compare Figs. 2 and 7.

The change in pH at the solution interface can be quantified further by computing $\Delta\text{pH}_{\text{out}}$ as defined in Eq. (17). From Fig. 5, we discern that for $\alpha \leq 0$, $\Delta\text{pH}_{\text{out}}$ as a function of the membrane curvature develops a local maximum whose position depends on the radius of the vesicle, R , contrary to the case of $\alpha \geq 0$ where $\Delta\text{pH}_{\text{out}}$ develops a local minimum as a function of the radius of the vesicle. In both cases, the position of the extremum also depends on the value of the interaction parameter χ displacing it towards the interface for larger positive values. The value of $\Delta\text{pH}_{\text{out}}$ can be either positive or negative, depending on the surface interaction parameters. For some combinations of (α , χ), $\Delta\text{pH}_{\text{out}}$ can show a second-order transition as a function of R , being zero for small enough R and then starting to deviate from zero at a critical value of the radius of the vesicle; see Fig. 6. This can only happen for large enough nearest-neighbor interactions at the surface, $\chi \neq 0$.

Another notable conclusion, following from the comparison between the DH approximation and the full PB solution, is that the former describes the same effects as the latter on a qualitative level. Notably, the DH approximation as used here does not imply just a DH solution for the electrostatic potential, but also a full minimization of the final free energy with nonlinear surface interaction terms included. It would probably be more appropriate to refer to it as the DH-CR solution than as merely a DH solution. We surmise that it could also be used to great advantage in other situations where the full PB solution is prohibitively difficult to find even numerically.

Last but not least, we need to clearly state that our model hinges on the assumption that the chemical potential of all the mobile species, the water dissociation products, the electrolyte ions and water, is constant, corresponding to the grand canonical ensemble. We therefore assume that during the

process of the vesicle formation, the chemical equilibrium is maintained at all times. If this were not the case, one could not define the Debye length through the bulk electrolyte concentration and one would have to formulate a canonical ensemble version of our model, where the process of vesicle formation traps a certain number of charged molecules inside the vesicle and the charge and density distributions would then strongly depend on the details of the vesicle formation process, precluding a detailed quantitative analysis since every preparation and indeed every vesicle in a single preparation could be characterized by a different amount of trapped charges.

ACKNOWLEDGMENTS

R.P., P.K. and H.R. acknowledge the support of the School of Physics, University of Chinese Academy of Sciences, Beijing, China. R.P. also acknowledges the support of the Wenzhou Institute of the University of Chinese Academy of Sciences, Wenzhou, Zhejiang, China. P.K., R.H. and R.P. acknowledge funding from the Grant No. 12034019 of the Key Project of the National Natural Science Foundation of China.

APPENDIX A: DEBYE-HÜCKEL SOLUTION

In the DH approximation, the electrostatic potential can be explicitly obtained for different regions of the problem [56]. Inside the vesicle,

$$\frac{1}{r} \frac{d^2[r\Phi_I(r)]}{dr^2} + \kappa_D^2 \Phi_I(r) = 0, \quad (\text{A1})$$

giving

$$\Phi_I(r \leq R) = A \frac{\sinh(\kappa_D r)}{r}. \quad (\text{A2})$$

In the lipid membrane or the amphiphilic layer, we have

$$\frac{1}{r} \frac{d^2[r\Phi_{II}(r)]}{dr^2} = 0, \quad (\text{A3})$$

implying

$$\Phi_{II}(R \leq r \leq R + w) = \frac{C}{r} + D, \quad (\text{A4})$$

while in the external compartment,

$$\frac{1}{r} \frac{d^2[r\Phi_{III}(r)]}{dr^2} + \kappa_D^2 \Phi_{III}(r) = 0 \quad (\text{A5})$$

is satisfied by

$$\Phi_{III}(r \geq R + w) = B \frac{\exp(-\kappa_D r)}{r}. \quad (\text{A6})$$

Here the inverse square of the Debye screening length is given by $\kappa_D^2 = 2n_I \beta e_0^2 / \epsilon_w \epsilon_0$, where n_I is the bulk electrolyte ionic concentration.

Above, we have obviously assumed that the two compartments (I and III) are in chemical equilibrium and can exchange electrolyte solution ions. If this were not the case, the screening properties, $\kappa_D(\text{I})$ and $\kappa_D(\text{III})$, would differ.

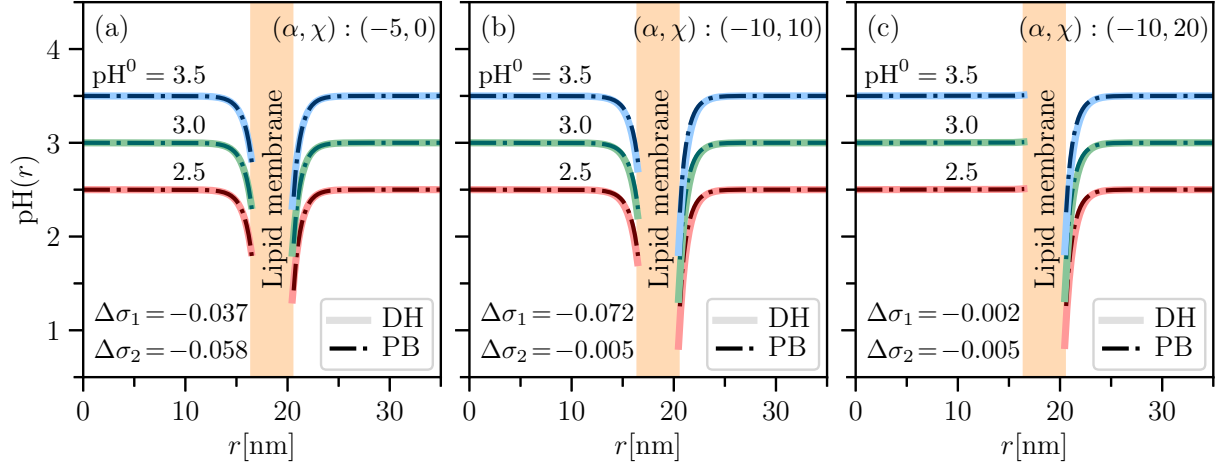


FIG. 8. Comparison of the spatial dependence of $\text{pH}(r)$ across the membrane for different values of the bulk pH^0 obtained from the full PB and the linearized DH solutions in the case of $\alpha \leq 0$. (a) $(\alpha, \chi) = (-5, 0)$, (b) $(\alpha, \chi) = (-10, 10)$, (c) $(\alpha, \chi) = (-10, 20)$ for different values of the bulk pH^0 . Here, $\Delta\sigma_i = \sigma_i^{\text{PB}} - \sigma_i^{\text{DH}}$ in the unit of e_0/nm^2 and $n_0 = 1 \text{ nm}^{-2}$ is used. The absolute value of σ_i is greater within the full PB theory, but it changes when there is a symmetry breaking, i.e., for $(\alpha, \chi) = (-10, 20)$. $\Delta\sigma_1$ is negative here, but σ_1 is positive in this case, implying that $\sigma_1^{\text{PB}} < \sigma_1^{\text{DH}}$. The largest discrepancies are observed in the vicinity of the membrane, but even then they are overall small and cannot be discerned on the scale of the figure.

The electrostatic potentials in different regions are connected via boundary conditions that have the standard form

$$\epsilon_w \left. \frac{\partial \Phi_{\text{I}}(r)}{\partial r} \right|_{r=R} - \epsilon_p \left. \frac{\partial \Phi_{\text{II}}(r)}{\partial r} \right|_{r=R} = \frac{\sigma_1}{\epsilon_0} \quad (\text{A7})$$

and

$$\epsilon_p \left. \frac{\partial \Phi_{\text{II}}(r)}{\partial r} \right|_{r=R+w} - \epsilon_w \left. \frac{\partial \Phi_{\text{III}}(r)}{\partial r} \right|_{r=R+w} = \frac{\sigma_2}{\epsilon_0}. \quad (\text{A8})$$

The four unknown coefficients, A , B , C , and D , are obtained from the boundary conditions and have the form obtained previously in [56]:

$$A = \mathcal{A}/\Delta, \quad B = \mathcal{B}/\Delta, \quad C = \mathcal{C}/\Delta, \quad D = \mathcal{D}/\Delta, \quad (\text{A9})$$

where

$$\begin{aligned} \Delta = & \epsilon_0 \epsilon_w \{ (\epsilon_p - \epsilon_w) \kappa_D w^2 + \epsilon_p \kappa_D R^2 \\ & + [\epsilon_p (1 + 2\kappa_D R) - \epsilon_w (1 + \kappa_D R)] w + \kappa_D R \\ & \times [\epsilon_w w^2 \kappa_D + \epsilon_p R + \epsilon_w (1 + \kappa_D R) w] \coth(\kappa_D R) \} \end{aligned} \quad (\text{A10})$$

and

$$\begin{aligned} \mathcal{A} = & \epsilon_w \sigma_1 R^2 \kappa_D w^2 + \epsilon_p [\sigma_1 R^2 + \sigma_2 (R + w)^2] R \\ & + \epsilon_w \sigma_1 (1 + \kappa_D R) w R^2 \text{csch}(\kappa_D R), \\ \mathcal{B} = & [\{ \epsilon_p (\sigma_1 R^2 + \sigma_2 (R + w)^2) - \epsilon_w \sigma_2 (R + w)^2 \} w \\ & + \epsilon_p [\sigma_1 R^2 + \sigma_2 (R + w)^2] R \\ & + \epsilon_w \sigma_2 (R + w)^2 \delta \kappa_D R \coth(\kappa_D R)] \exp[\kappa_D (R + w)], \\ \mathcal{C} = & \epsilon_w \{ \sigma_1 w^2 \kappa_D R^2 + [\sigma_1 R^2 + \sigma_2 (R + w)^2] R \\ & + \sigma_1 R^2 (1 + 2\kappa_D R) w \\ & - \sigma_2 (R + w)^2 \kappa_D \coth(\kappa_D R) \}, \end{aligned}$$

$$\begin{aligned} \mathcal{D} = & \epsilon_p [\sigma_1 R^2 + \sigma_2 (R + w)^2] \\ & - \epsilon_w [\sigma_1 R^2 + \sigma_2 (R + w)^2 + \sigma_1 R^2 \kappa_D (R + w)] \\ & + \epsilon_w \kappa_D \sigma_2 (R + w)^2 R \coth(\kappa_D R). \end{aligned} \quad (\text{A11})$$

The results quoted in the main text are based on the various limits stemming from these expressions.

APPENDIX B: COMPARISON BETWEEN THE FULL POISSON-BOLTZMANN AND THE APPROXIMATE DEBYE-HÜCKEL SOLUTIONS

Here we compare the linearized DH solution with the full numerical solution of the PB equation. Technically, this refers to solutions of the full PB equation,

$$\frac{1}{r} \frac{d^2[r\Phi(r)]}{dr^2} + \frac{\kappa_D^2}{\beta e_0} \sinh \beta e_0 \Phi(r) = 0, \quad (\text{B1})$$

and the linearized DH equation,

$$\frac{1}{r} \frac{d^2[r\Phi(r)]}{dr^2} + \kappa_D^2 \Phi(r) = 0, \quad (\text{B2})$$

in the regions (I and III) accessible to the electrolyte ions. The methodology for obtaining the PB numerics has been explained in detail in our previous publications [20–22] and will not be elaborated here.

In Figs. 8 and 9, we compare the spatial profile of the pH as obtained from the PB and the DH solutions. We notice that overall, the difference for the chosen values of the parameters is small, but is smaller for $\alpha \leq 0$ (Fig. 8) than for $\alpha \geq 0$ (Fig. 9). In fact, for large positive α , the DH solution ceases to be a good approximation for the PB result, which would invalidate the DH approach. We also specifically indicate the difference in the surface charge densities, $\Delta\sigma_i = \sigma_i^{\text{PB}} - \sigma_i^{\text{DH}}$, obtained from the two approaches in order to facilitate the comparison.

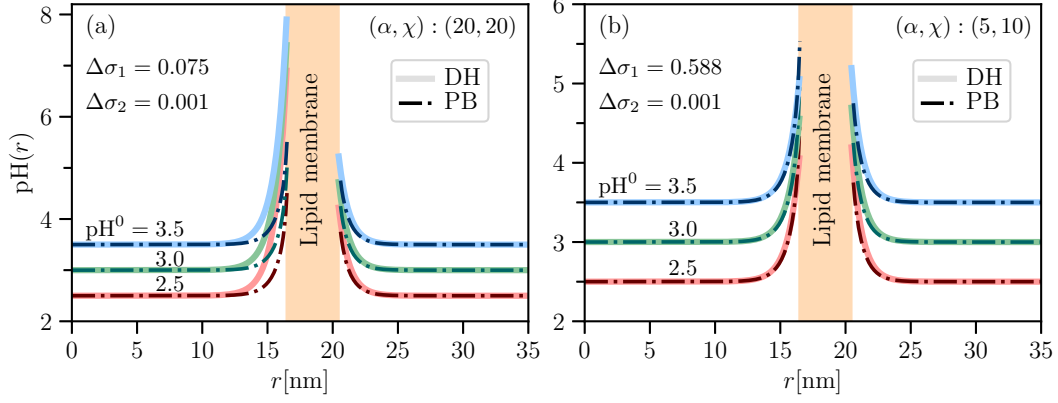


FIG. 9. Comparison of the spatial dependence of $\text{pH}(r)$ across the membrane for different values of the bulk pH^0 obtained from the full PB and the linearized DH solutions in the case of $\alpha \geq 0$. (a) $(\alpha, \chi) = (20, 20)$, (b) $(\alpha, \chi) = (5, 10)$, and $\Delta\sigma_i = \sigma_i^{\text{PB}} - \sigma_i^{\text{DH}}$ is provided in the unit of e_0/nm^2 . For all the plots, $n_0 = 1 \text{ nm}^{-2}$ is considered. One observes a significant deviation between pH values obtained from PB and DH approaches for $(\alpha, \chi) = (20, 20)$. For $(\alpha, \chi) = (5, 10)$, the difference is nevertheless small although $\Delta\sigma_1$ is higher in this case. This is because of the value of σ_1 itself, which is high for $(\alpha, \chi) = (20, 20)$.

One conclusion following from the numerical results of the PB and DH approaches is that qualitatively, they are very similar, but for certain values of the parameters, there are quantitative differences. It seems that one can thus safely use the DH approximation if the focus is on the qualitative features, whereas a PB-based calculation would be needed in order to do quantitative comparisons.

Concerning the quantitative mismatch between the PB and DH theories, we see the same trends as reported earlier [25]. For equal surface charge densities, linear DH theory overestimates the electrostatic potential. As our current study suggests, this remains true even when charge regulation is included, unless the surface charge densities computed within the two theories do not vary too much. For significantly larger $\Delta\sigma_i$, as is the case for the luminal region in Fig. 9(b), the electrostatic potential and the corresponding pH can, of course, be larger for the PB theory.

APPENDIX C: CURVATURE EXPANSION PARAMETERS

In writing the DH electrostatic free energy in the curvature expanded form, given by Eq. (7) (see [24] for details), which is based on the solution of the DH equation [56], we introduced the following quantities:

$$f_0(\sigma_1, \sigma_2, \kappa_D, w) = \frac{\mu(\sigma_1 + \sigma_2)^2 + \kappa_D w(\sigma_1^2 + \sigma_2^2)}{2\mu + \kappa_D w}, \quad (\text{C1})$$

$$\begin{aligned} f_1(\sigma_1, \sigma_2, \kappa_D, w) \\ = \kappa_D w \left(\frac{[3\mu + 2(\kappa_D w) - 1]\sigma_2^2 + 2\mu\sigma_1\sigma_2 - (\mu - 1)\sigma_1^2}{2\mu + (\kappa_D w)} \right), \end{aligned} \quad (\text{C2})$$

and

$$\begin{aligned} f_2(\sigma_1, \sigma_2, \kappa_D, w) = \frac{\kappa_D w}{[2\mu + (\kappa_D w)]^2} \{ (\mu - 1)[(\kappa_D w)(\mu - 1) - \mu]\sigma_1^2 - 2\mu[(\kappa_D w) + 1](\mu - 1)\sigma_1\sigma_2 \\ + [(\kappa_D w)^3 + (\kappa_D w)^2(4\mu - 1) + (\kappa_D w)(5\mu^2 - 4\mu + 1) - \mu(\mu - 1)]\sigma_2^2 \}, \end{aligned} \quad (\text{C3})$$

which no longer depend on the curvature of the membrane. In addition, for the curved membrane, f_0 , f_1 , and f_2 are not symmetric with respect to the two solvent accessible inner and outer surface charge densities.

APPENDIX D: DEPENDENCE OF ΔpH_m , ΔpH_w , $\Delta\text{pH}_{\text{out}}$ ON CURVATURE

Taking into account the DH solution for Φ_I , Φ_{II} , and Φ_{III} above, and the definition of the constants $A = A(R, w)$, $B = B(R, w)$, and $C = C(R, w)$ in Eq. (A11) that explicitly depend on R , w , we can rewrite the equations for the changes of the

acidity, Eqs. (16)–(18), in the explicit form

$$\begin{aligned} \Delta\text{pH}_m &= \text{pH}(R + w) - \text{pH}(R) \\ &= \beta e_0 \log_{10} e \left[B(R, w) \frac{\exp[-\kappa_D(R + w)]}{(R + w)} \right. \\ &\quad \left. - A(R, w) \frac{\sinh(\kappa_D R)}{R} \right], \end{aligned} \quad (\text{D1})$$

$$\begin{aligned} \Delta\text{pH}_{\text{out}} &= \text{pH}(r = R + w) - \text{pH}^0 \\ &= \beta e_0 \log_{10} e B(R, w) \frac{\exp[-\kappa_D(R + w)]}{R + w}, \end{aligned} \quad (\text{D2})$$

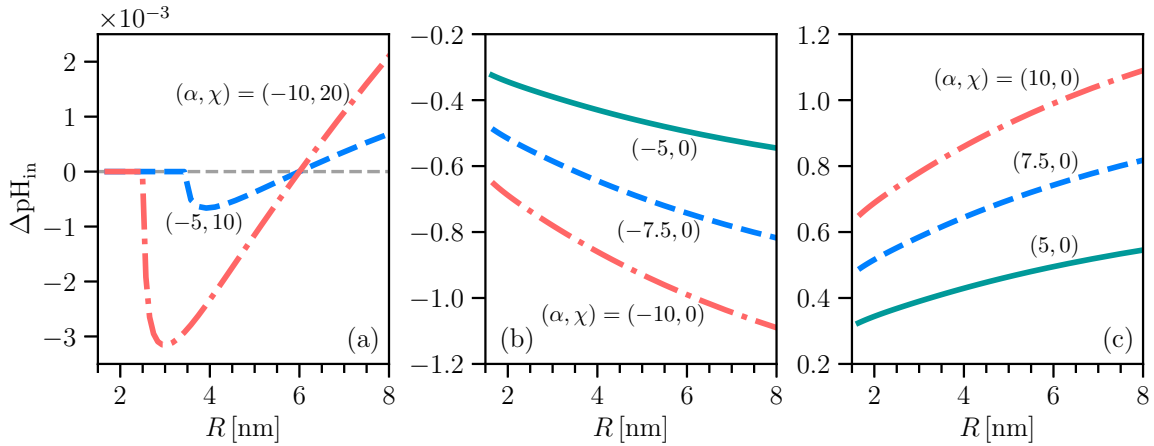


FIG. 10. Plot of $\Delta\text{pH}_{\text{in}}$ vs R for (a) the “critical isotherm” $\chi = -2\alpha$ case, and for $\chi = 0$ for (b) negative and (c) positive values of α . Overall, $\Delta\text{pH}_{\text{in}}$ is very small with different behaviors in a curve, i.e., (i) $\Delta\text{pH}_{\text{in}} < 0$, (ii) $\Delta\text{pH}_{\text{in}} = 0$, and (iii) $\Delta\text{pH}_{\text{in}} > 0$, i.e., $\Delta\text{pH}_{\text{in}}$ can increase, decrease, or remain constant as the radius R varies. (b), (c) Plots of $\Delta\text{pH}_{\text{in}}$ vs R for the $\chi = 0$ case, which corresponds to no surface interaction. Plots are for (b) $\alpha < 0$ and (c) $\alpha > 0$. The $\Delta\text{pH}_{\text{in}}$ in both cases are, in fact, the same in absolute value, but different in sign. For all cases, $\kappa_D = 1.215 \text{ nm}^{-1}$.

and

$$\begin{aligned} \Delta\text{pH}_{\text{in}} &= \text{pH}(r = R) - \text{pH}^0 \\ &= \beta e_0 \log_{10} e A(R, w) \frac{\sinh(\kappa_D R)}{R}. \end{aligned} \quad (\text{D3})$$

Figures 10 and 11 show the plots of $\Delta\text{pH}_{\text{in}}$ vs R , with the rest of the parameters the same as before. Figure 11 shows that $\Delta\text{pH}_{\text{in}}$ decreases when we increase the size of the vesicle for $\alpha < 0$ [Fig. 11(a)], while $\Delta\text{pH}_{\text{in}}$ increases when the size of the

vesicle increases for $\alpha > 0$ [Fig. 11(b)]. In addition, in Fig. 10, we found that the dependence of $\Delta\text{pH}_{\text{in}}$ on the radius R can show an increase, decrease, or remain constant, depending on the values of the parameters (α, χ) . What is particularly interesting is the “critical isotherm” corresponding to the $\chi = -2\alpha$ case that shows no variation with radius up to a critical value and, after that, a nonmonotonic dependence. Figure 10 shows the case of $\chi = 0$ (no surface interaction). The plots are for both $\alpha < 0$ [Fig. 10(b)] and $\alpha > 0$ [Fig. 10(c)]. We found that the $\Delta\text{pH}_{\text{in}}$ are the same, but different in sign.

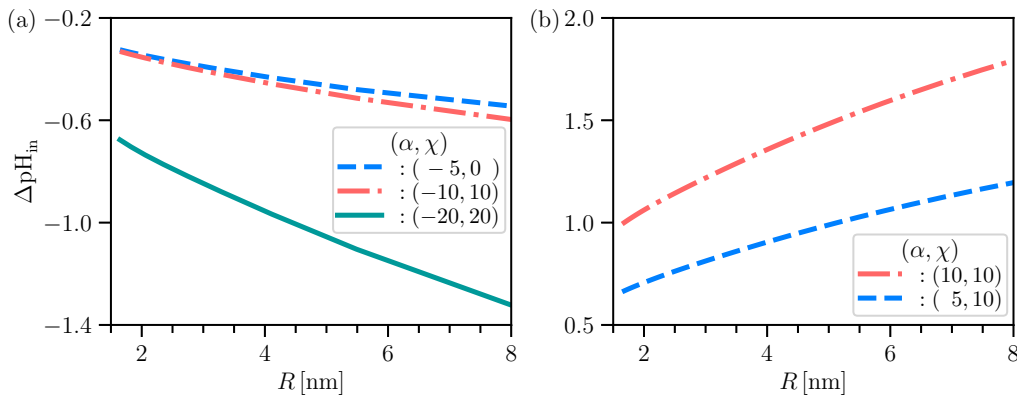


FIG. 11. Plot of $\Delta\text{pH}_{\text{in}}$ vs R . The inverse Debye length κ_D is fixed at 1.215 nm^{-1} . σ_1 and σ_2 are obtained from the CR process. The plots are shown for (a) $\alpha < 0$ and (b) $\alpha > 0$. $\Delta\text{pH}_{\text{in}}$ (a) decreases or (b) increases when the size of the vesicle increases.

- [1] G. Cevc, in *Encyclopedia of Biophysics*, edited by G. C. K. Roberts and A. Watts (Springer, Berlin, 2018), pp. 1446–1452.
- [2] V. P. Zhdanov, *Eur. Biophys. J.* **52**, 121 (2023).
- [3] K. Holmberg, B. Jönsson, B. Kronberg, and B. Lindman, *Surfactants and Polymers in Aqueous Solution* (Wiley, England, 2002), pp. 1–525.
- [4] H.-X. Zhou and X. Pang, *Chem. Rev.* **118**, 1691 (2018).
- [5] T. Simonson, *Rep. Prog. Phys.* **66**, 737 (2003).
- [6] R. J. Nap, A. L. Božič, I. Szleifer, and R. Podgornik, *Biophys. J.* **107**, 1970 (2014).
- [7] V. V. Galassi and N. Wilke, *Membranes* **11**, 478 (2021).
- [8] P. Khunpetch, A. Majee, and R. Podgornik, *Soft Matter* **18**, 2597 (2022).
- [9] G. Cevc, *Biochim. Biophys. Acta* **1031**, 311 (1990).

- [10] V. Panagiotopoulou, A theoretical and experimental study of cell membrane electrostatics and transport, Ph.D. thesis, University of Nottingham, 2012.
- [11] Y. Sarkar, R. Majumder, S. Das, A. Ray, and P. P. Parui, *Langmuir* **34**, 6271 (2018).
- [12] R. Zandi, B. Dragnea, A. Travesset, and R. Podgornik, *Phys. Rep.* **847**, 1 (2020).
- [13] L. Javidpour, A. Božič, A. Naji, and R. Podgornik, *Soft Matter* **17**, 4296 (2021).
- [14] D. Roshal, O. Konevtsova, A. Lošdorfer Božič, R. Podgornik, and S. Rochal, *Sci. Rep.* **9**, 5341 (2019).
- [15] O. V. Konevtsova, D. S. Roshal, A. Lošdorfer Božič, R. Podgornik, and S. Roshal, *Soft Matter* **15**, 7663 (2019).
- [16] S. B. Rochal, O. V. Konevtsova, D. S. Roshal, A. Božič, I. Y. Golushko, and R. Podgornik, *Nanoscale Adv.* **4**, 4677 (2022).
- [17] G. S. Longo, M. Olvera de la Cruz, and I. Szleifer, *Macromolecules* **44**, 147 (2011).
- [18] G. S. Longo, M. Olvera de la Cruz, and I. Szleifer, *ACS Nano* **7**, 2693 (2013).
- [19] M. I. Angelova, A.-F. Bitbol, M. Seigneuret, G. Staneva, A. Kodama, Y. Sakuma, T. Kawakatsu, M. Imai, and N. Puff, *Biochim. Biophys. Acta (BBA)* **1860**, 2042 (2018).
- [20] A. Majee, M. Bier, and R. Podgornik, *Soft Matter* **14**, 985 (2018).
- [21] A. Majee, M. Bier, R. Blossey, and R. Podgornik, *Phys. Rev. E* **100**, 050601(R) (2019).
- [22] A. Majee, M. Bier, R. Blossey, and R. Podgornik, *Phys. Rev. Res.* **2**, 043417 (2020).
- [23] B. W. Ninham and V. A. Parsegian, *J. Theor. Biol.* **31**, 405 (1971).
- [24] H. R. Shojaei, A. L. Božič, M. Muthukumar, and R. Podgornik, *Phys. Rev. E* **93**, 052415 (2016).
- [25] A. Majee, M. Bier, and S. Dietrich, *J. Chem. Phys.* **145**, 064707 (2016).
- [26] R. Bebon and A. Majee, *J. Chem. Phys.* **153**, 044903 (2020).
- [27] S. V. Siryk, A. Bendandi, A. Diaspro, and W. Rocchia, *J. Chem. Phys.* **155**, 114114 (2021).
- [28] S. V. Siryk and W. Rocchia, *J. Phys. Chem. B* **126**, 10400 (2022).
- [29] T. Markovich, D. Andelman, and R. Podgornik, in *Handbook of Lipid Membranes*, edited by C. R. Safynia and J. O. Raedler (Taylor & Francis, London, 2021), pp. 99–128.
- [30] M. Muthukumar, *Physics of Charged Macromolecules. Synthetic and Biological Systems* (Cambridge University Press, Cambridge, 2023).
- [31] D. Andelman, in *Handbook of Biological Physics: Structure and Dynamics of Membranes*, edited by R. Lipowsky and E. Sackmann (Elsevier, Amsterdam, 1995), pp. 603–642.
- [32] A. Fogden and B. Ninham, *Adv. Colloid Interface Sci.* **83**, 85 (1999).
- [33] E. J. Verwey and J. T. G. Overbeek, *Theory of the Stability of Lyophobic Colloids* (Elsevier, Amsterdam, 1948).
- [34] M. Winterhalter and W. Helfrich, *J. Phys. Chem.* **92**, 6865 (1988).
- [35] D. J. Mitchell and B. W. Ninham, *Langmuir* **5**, 1121 (1989).
- [36] H. Lekkerkerker, *Physica A* **167**, 384 (1990).
- [37] B. Duplantier, R. E. Goldstein, V. Romero-Rochin, and A. I. Pesci, *Phys. Rev. Lett.* **65**, 508 (1990).
- [38] J. L. Harden, C. Marques, J. F. Joanny, and D. Andelman, *Langmuir* **8**, 1170 (1992).
- [39] L. Koopal, W. Tan, and M. Avena, *Adv. Colloid Interface Sci.* **280**, 102138 (2020).
- [40] M. Borkovec, B. Jönsson, and G. J. M. Koper, in *Surface and Colloid Science*, edited by E. Matijević (Kluwer Academic/Plenum Publishers, New York, 2001), pp. 99–340.
- [41] D. Marsh, *Handbook of Lipid Bilayers*, 2nd ed. (CRC Press, Boca Raton, FL, 2013).
- [42] Y. Avni, T. Markovich, R. Podgornik, and D. Andelman, *Soft Matter* **14**, 6058 (2018).
- [43] N. Adžić and R. Podgornik, *Eur. Phys. J. E* **37**, 49 (2014).
- [44] I. Teraoka, *Polymer Solutions: An Introduction to Physical Properties* (Wiley, New York, 2002).
- [45] Y. Avni, R. Podgornik, and D. Andelman, *J. Chem. Phys.* **153**, 024901 (2020).
- [46] R. Podgornik, *J. Chem. Phys.* **149**, 104701 (2018).
- [47] D. Harries, R. Podgornik, V. A. Parsegian, E. Mar-Or, and D. Andelman, *J. Chem. Phys.* **124**, 224702 (2006).
- [48] Y. Avni, D. Andelman, and R. Podgornik, *Curr. Opin. Electrochem.* **13**, 70 (2019).
- [49] S. L. Carnie and D. Y. Chan, *J. Colloid Interface Sci.* **161**, 260 (1993).
- [50] R. Pericet-Camara, G. Papastavrou, S. H. Behrens, and M. Borkovec, *J. Phys. Chem. B* **108**, 19467 (2004).
- [51] J. Landsgesell, L. Nová, O. Rud, F. Uhlík, D. Sean, P. Hebbeker, C. Holm, and P. Košovan, *Soft Matter* **15**, 1155 (2019).
- [52] J. Landsgesell, P. Hebbeker, O. Rud, R. Lunkad, P. Košovan, and C. Holm, *Macromolecules* **53**, 3007 (2020).
- [53] T. Chou, M. V. Jarić, and E. D. Siggia, *Biophys. J.* **72**, 2042 (1997).
- [54] R. Majumder, Y. Sarkar, S. Das, A. Ray, and P. P. Parui, *New J. Chem.* **41**, 8536 (2017).
- [55] H. J. Muhren and P. van der Schoot, *J. Phys. Chem. B* **127**, 2160 (2023).
- [56] A. Šiber and R. Podgornik, *Phys. Rev. E* **76**, 061906 (2007).